ELSEVIER

Coordination Chemistry Reviews
196 (2000) 307–329

COORDINATION CHEMISTRY REVIEWS

www.elsevier.com/locate/ccr

Supramolecular assemblies of ruthenium complexes and porphyrins

Henrique E. Toma *, Koiti Araki

Instituto de Química-USP, C. Postal 26.077, CEP 05599-970 São Paulo, SP, Brazil

Contents

Abstract

The build-up of polymetallic supermolecules based on porphyrins and ruthenium bipyridine complexes has been pursued with great interest. A relevant series of symmetric polynuclear species has been obtained by attaching four $[Ru^{II}(bipy)_2Cl]$ groups to the pyridyl substituents of *meso*-tetra(4-pyridyl)porphyrin and its metallated derivatives. These compounds display a rich electrochemistry and versatile catalytic and photochemical properties, associated with the ruthenium–bipyridine and metalloporphyrin complexes. The supermolecular species interact very strongly with DNA, yielding by irradiation with visible light, very efficient single-strand breaks and formation of 8-oxo-7,8-dihydroxo-2′-deoxyguanosine.

* Corresponding author. Tel.: +55-11-8183887; fax: +55-11-8155579.
E-mail address: henetoma@quim.iq.usp.br (H.E. Toma)

PII: S0010-8545(99)00041-7

Another interesting property of the supramolecular porphyrins is their ability to form homogeneous and adherent molecular films by dip-coating. When combined with anionic porphyrins, self-assembled films can be generated, layer-by-layer, in a controlled way. Both types of films display photoaction response in the presence of visible light. The modified electrodes exhibit rectifying response in the presence of reducing species, demonstrating excellent performance as FIA detectors for biological and environmentally relevant substrates such as dopamine, NADH, ascorbic acid and sulfite ions.

Keywords: FIA; Polynuclear porphyrins; Supramolecular assembly; Thin films

1. Introduction

Supramolecular chemistry involves the assembly of organized entities, by means of the association of two or more molecular entities through covalent bonds, electrostatic forces or weak van der Waals interactions. An infinite number of possibilities arises from the great variety of known chemical species; however, the build-up of supramolecular assemblies based on coordination compounds provides a unique and rather attractive approach, allowing for instance the exploitation of the metal–ligand affinities to build complex architectures for molecular recognition and self-assembly purposes. In fact, because of the intrinsic similarities and strategies involved, Lehn [1] has already mentioned that supramolecular chemistry can be regarded as a generalization of coordination chemistry.

The supramolecular assembly approach based on coordination compounds is primarily directed by the metal–ligand affinities, stereochemistry and substitution properties of the complexes involved. Along this line, a series of symmetric heptanuclear species has been generated by the coordination of $[Fe(CN)_5]^{3-}$, $[Ru(NH_3)_5]^{2+}$ and $[Ru(edta)]^{-}$ groups to the six external nitrogen atoms of the tris(bipyrazine)ruthenium(II) complex, $[Ru(bpz)_3]^{2+}$ [2–5]. In all of them, the luminescence of the $[Ru(bpz)_3]^{2+}$ chromophore was completely quenched by the peripheral metal complexes, via intramolecular electron transfer in the excited state. However, the Prussian blue film formed with $[Ru^{II}(bpz)_3\{Fe(CN)_5\}_n]^{m-}$ was shown to be photoelectrochemically active and the photoaction spectrum was similar to the absorption spectrum of the $[Ru^{II}(bpz)_3]^{2+}$ center [6].

Ruthenium clusters of the type $[Ru_3O(OOCCH_3)_6L_3]$ exhibit a triangular structure, strongly held by acetate and μ-oxo-bridges as well as by metal–metal bonds [7–12]. Supramolecular clusters have been assembled by binding $[Ru(NH_3)_5]^{2+}$, $[Ru(edta)]^{2-}$ and $[Fe(CN)_5]^{3-}$ groups to the Ru_3O core, via pyrazine or 4,4′-bipyridine bridging ligands, leading to hexanuclear complexes. Recently, tetrameric clusters have been obtained [8,9] by the reaction of a symmetric $[Ru_3O(OOCCH_3)_6L_3]^{+}$ cluster containing a bridging ligand (L = pyrazine, or 4,4′-bipyridine) and $[Ru_3O(OOCCH_3)_6(py)_2]^{+}$ as terminal groups.

Another interesting series of polynuclear ruthenium complexes incorporating up to 13 metal centers has been reported by Balzani et al. [13–19]. These complexes are

based on 2,5-bis(2-pyridyl)pyrazine as a bidentate bridging ligand and 2,2′-bipyridine in the terminal positions. The use of bidentate ligands leads to the formation of many isomers, complicating the studies of energy or electron transfer processes. This problem has been circumvented by employing tridentate polypyridine ligands with rigid spacers in order to bring together electron or energy donor and acceptor groups, generating dyads, tryads, etc. [20–27].

2. Polyruthenated porphyrins

From the myriad of interesting supramolecular systems that have been reported in the literature [28], we will mainly focus on a remarkable series constituted by porphyrins and ruthenium complexes, which has been systematically investigated in our laboratory over the last 10 years. The interest in this type of supramolecular porphyrin species has increased dramatically in the recent years, especially after the discovery of the exceptional electrocatalytic efficiency of the penta-amineruthenium–cobalt porphyrin species in the four-electron reduction of molecular oxygen [29–31].

Porphyrins are important prosthetic groups for a number of metalloproteins and enzymes, and their function depends on the metal ion and the nature of the axial ligands, as well as on the specific environment provided by the polypeptide chain. On the other hand, ruthenium polypyridine complexes represent one of the most important classes of coordination compounds displaying a very rich redox and photochemical character. The combination of the two types of complex provides a good opportunity to generate a novel series of mixed porphyrin–rutheniumpolyimine compounds, allowing the exploitation of their supramolecular properties, particularly for applications in catalysis, artificial photosynthesis and molecular devices. Illustrative cases have already been reported by Sessler et al. [32], consisting

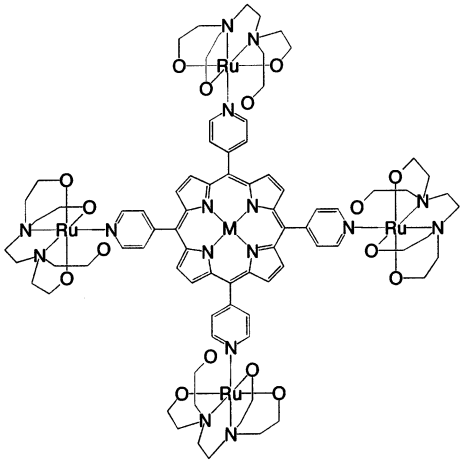

Fig. 1. Structural representation of the polymetallic porphyrin $[M–TPyP\{Ru(edta)\}_4]^{n+}$.

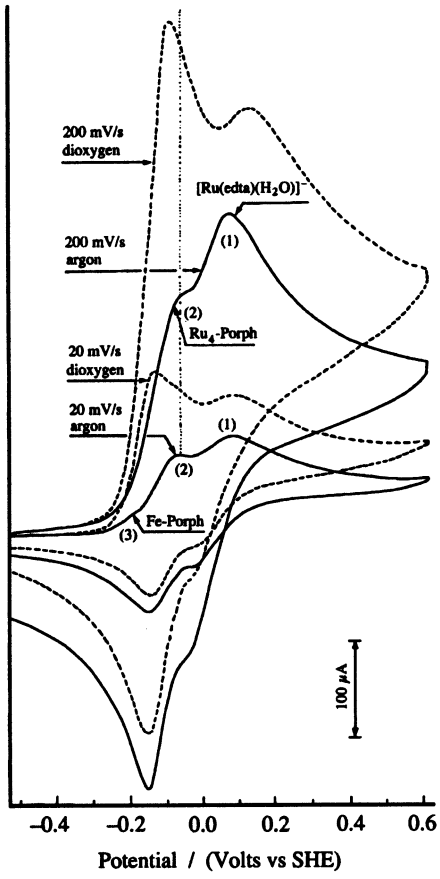

Fig. 2. Cyclic voltammograms of the $[Fe^{III}TPyP\{Ru^{III}(edta)\}_4]$ complex, 1.8×10^{-3} mol dm^{-3}, in argon or dioxygen saturated solutions, showing the catalytic peak at -0.1 V. $[Ru(edta)(H_2O)] = 1.8 \times 10^{-3}$ mol dm^{-3}, $[KCl] = 0.50$ mol dm^{-3}, pH 4.5 (acetate buffer, 0.05 mol dm^{-3}), glassy carbon electrode, 25°C.

of mono and bis-*meso*-2,2′-bipyridine substituted porphyrins attached to $[Ru(bipy)_2]^{2+}$ moieties, as well as by Sauvage and coworkers [33–36], dealing with linear porphyrins with mono- and 5,15-di-4′-*p*-phenyl-2,2′:6′,2″-terpyridine substituted porphyrins as tridentate sites bound to ruthenium(II) ions.

meso-(4-Pyridyl)porphyrins (TPyP) containing four ruthenium complexes attached to the peripheral pyridine groups have been investigated in our laboratory. The first system investigated was reported in 1988, consisting of TPyP bound to $[Ru(NH_3)_5]^{2+}$ groups [37]. A related species, containing four $[Ru^{III}(edta)]^-$ groups (see Fig. 1), i.e. $[M–TPyP\{Ru^{III}(edta)\}_4]^{4-}$ where M = Fe or Co [38,39], was reported soon after. The supramolecular assembly was planned in order to enhance the catalytic activity of the metalloporphyrin site. In both systems, the peripheral ruthenium(II) complexes were expected to act as electron sources, transferring

rapidly up to four electrons to the reactive center. In fact, an enhanced electrocatalytic activity in the four electron reduction reaction of molecular oxygen [38] (see Fig. 2) was observed for the $[Fe–TPyP\{Ru(edta)\}_4]^{4-}$ complex. Resonance Raman studies were carried out to confirm the existence of electronic coupling between the $[Ru^{II}(edta)]$ complex and the porphyrin core [40].

The dioxygen reduction by this type of polymetallic porphyrins was extensively investigated by Anson and coworkers [29–31,41–43] with particular emphasis on cobalt *meso*-(4-pyridyl) and *meso*-(4-cyanophenyl)porphyrins coordinated to $Ru(NH_3)_5$ groups. A remarkable result was obtained with [Co–TPyP] coordinated to four $[Ru(NH_3)_5]^{2+}$ complexes. This species was generated in situ, onto pyrolitic graphite electrodes, and exhibited pronounced electrocatalytic activity for the tetraelectronic reduction of O_2. This behavior was attributed to the back-bonding effect of the Ru(II) complexes on the cobalt porphyrin active site.

More recently, a new generation of tetraruthenated porphyrins has been pursued, incorporating photochemically and electrochemically active groups to the porphyrin system. The prototype system in this series consists of *meso*-tetra(4-pyridyl)porphyrin containing four $[Ru(bipy)_2Cl]^+$ groups as modifiers [44], as shown in Fig. 3, and will be denoted TRP (tetraruthenated porphyrin).

It should be mentioned that the binding of asymmetric groups to the tetrapyridylporphyrin ring, as in Figs. 1 and 3, can lead to a number of diastereoisomers. However, the chemical environment around the peripheral groups is rather similar. From the point of view of their spectroscopic, electrochemical and photochemical properties, the diastereoisomers can not be distinguished, behaving, therefore, as a pure compound.

The electronic spectra of this species exhibit the characteristic porphyrin Soret band at 418 nm and the β and α doublets at 518, 558 and 594, 650 nm, respectively,

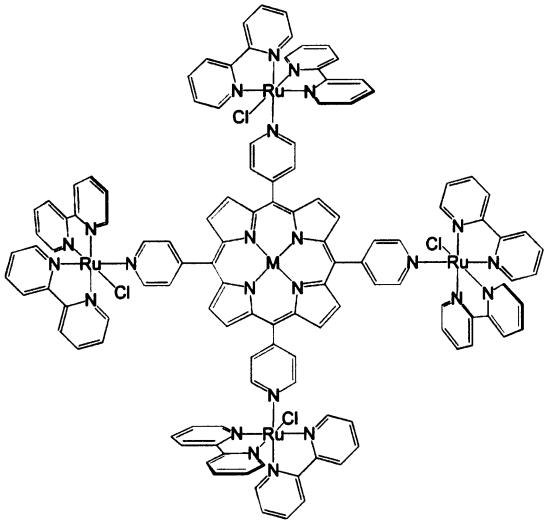

Fig. 3. Structural representation of $[TPyP\{Ru(bipy)_2Cl\}_4]^{4+}$ complex, TRP.

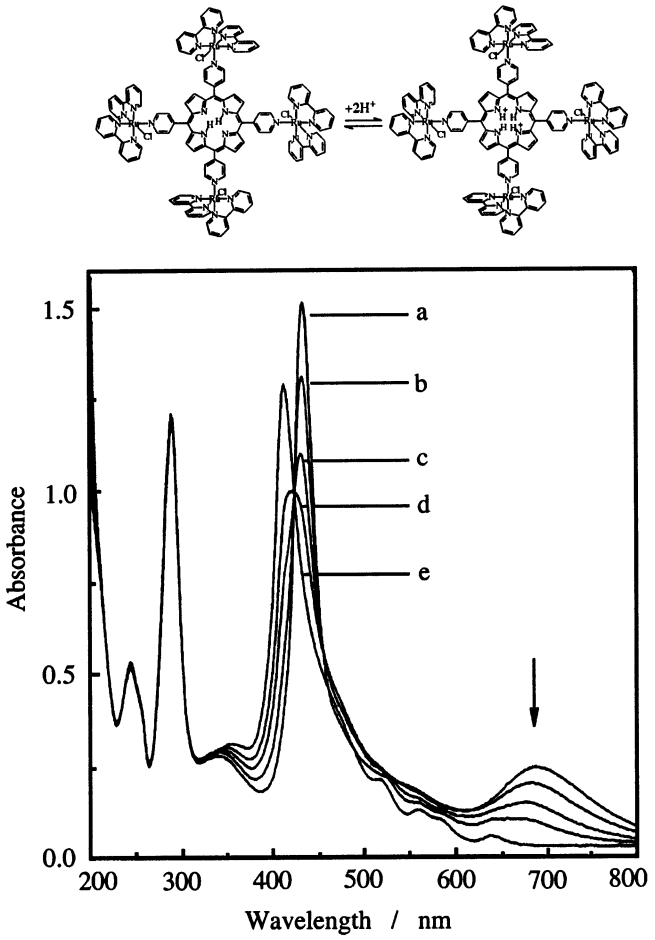

Fig. 4. Electronic spectra of aqueous solutions of 5.8 μM [TRP]Cl_4 at pH: (a) 1.24; (b) 1.71; (c) 1.98; (d) 2.2 and (e) 5.30. Top: acid/base reaction of TRP, showing the structure of the free-base and protonated species.

in addition to the absorption bands of the $[Ru(bipy)_2Cl]^+$ moieties at 298 nm (bipy $\pi \rightarrow \pi^*$) and 470 nm (Ru^{II}(bipy charge-transfer) [45]. The complex emits at 655 and 700 nm (sh), when excited at the porphyrin or $[Ru(bipy)_2Cl]^+$ absorption bands. The emission energies, fluorescence and excited state spectra are similar to those observed for (tetra-*N*-methylpyridinium)porphyrin, indicating that the fluorescence and the lowest triplet excited state are localized on the porphyrin center. The excitation spectrum reproduces the absorption spectrum of the tetraruthenated porphyrin, even in the region of the $[Ru(bipy)_2Cl]^+$ chromophore. Therefore, the π^* emitting state can be pumped either from a direct excitation at the porphyrin center, or by an intramolecular energy transfer mechanism from the peripheral ruthenium complexes.

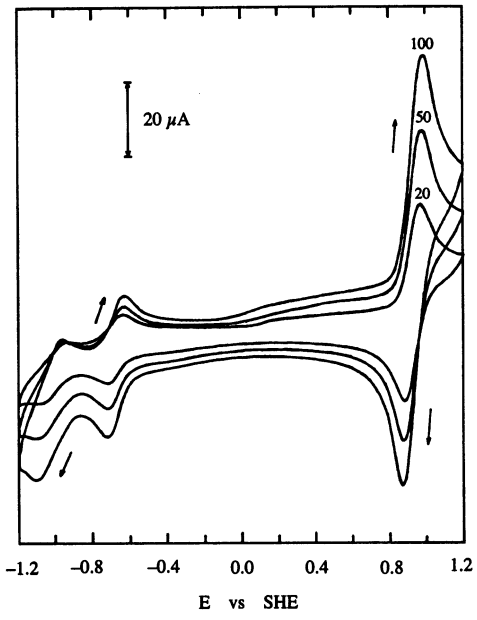

Fig. 5. Cyclic voltammograms of 1.2 mM [TRP](PF)$_6$ in DMF, 0.10 M TEAPF$_6$.

Below pH 3, the modified porphyrin can be reversibly protonated at the pyrrole N-atoms, shifting the Soret band from 414 to 440 nm, as illustrated in Fig. 4. The absorption bands of the peripheral ruthenium complexes remain practically unchanged, however a new intense band appears around 690 nm, exhibiting a systematic decay when the metal ions are oxidized or when the porphyrin is reduced. Based on the spectroelectrochemical behavior, this band has been assigned as a ruthenium(II)-to-protonated porphyrin charge-transfer transition.

Cyclic voltammograms of the tetrametallated porphyrin $[TPyP\{Ru(bipy)_2Cl\}_4]^{4+}$ species exhibit reversible waves at 0.92, -0.68 and -0.93 V, the first one being four times more intense than the other two, as shown in Fig. 5. The spectroelectrochemical measurements at 0.92 V reveal reversible changes in the absorption bands at 470 and 298 nm, associated with the MLCT and $\pi \rightarrow \pi^*$ bands in the $[Ru(bipy)_2Cl]^+$ chromophore, supporting the oxidation of the ruthenium complexes. This process leads to a 30% increase in the intensity of the Soret band, which is shifted from 418 to 424 nm, reflecting the perturbation of the electronic levels of TPyP by the ruthenium complexes. The spectroelectrochemical behavior at –0.68 and –0.93 V is similar to that observed for $TMPyP^{4+}$ and consistent with two successive monoelectronic redox processes at the porphyrin ring, showing a complete decay of the Soret band.

Similar spectroscopic and electrochemical properties [46] were observed for $[TPyP\{Ru(phen)_2Cl\}_4]^{4+}$. The fluorescence spectrum exhibits two intense bands at 660 and 710 nm in contrast with TRP, where the higher energy band predominates.

3. Tetraruthenated metalloporphyrins

The presence of the metal ion is known to have a dramatic effect on the properties of the metalloporphyrins, in addition to its major role as a reactive or catalytic center. In spite of their very similar structures, the chemistry of the zinc, cobalt or iron porphyrins, for instance, is quite distinct, reflecting the nature of the transition metal center modulated by the strong field macrocyclic environment. For this reason, from the point of view of the chemistry involved, each metalloporphyrin species deserves special attention. In addition, the supramolecular assembly based on transition metal complexes introduces a number of specific electronic or molecular interactions to be exploited for each metalloporphyrin system.

The electrochemistry of the series of tetraruthenated metalloporphyrins, M–TRP, is indeed very rich. In acetonitrile solutions, up to 16 electrons can be added or removed in the potential range of -1.8 to 1.6 V. The complexes of ruthenium(II) with 2,2′-bipyridine can be oxidized to the corresponding ruthenium(III) complexes, and each bipy ligand can be reduced by the successive addition of electrons. Likewise, the porphyrin ring can be either oxidized or reduced, generating the cation radical and its corresponding dication, or the anion radical and its corresponding dianion. In addition, the central ion can also be electrochemically active, but in this case, its properties will be strongly dependent on the supramolecular environment. Because of the presence of several electroactive groups exhibiting

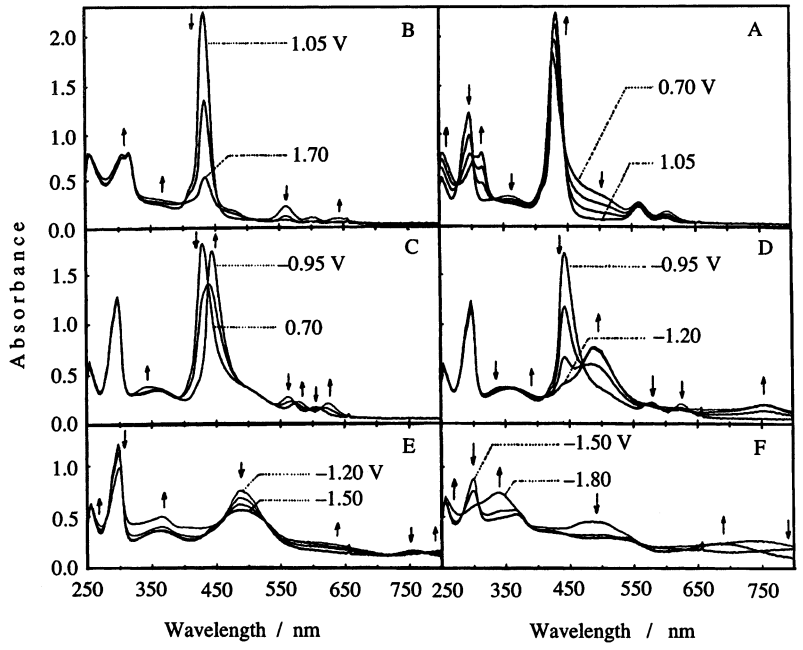

Fig. 6. Spectroelectrochemistry of [Zn–TRP](TFMS)$_4$ (2.0×10^{-4} M) in DMF (0.10 M TEAClO$_4$) at: (A) 0.70–1.05 V; (B) 1.05–1.70 V; (C) 0.70 to -0.95 V; (D) -0.95 to -1.20 V; (E) -1.20 to -1.50 V and (F) -1.50 to -1.80 V.

closely related redox potentials, in many cases the assignment of the electrochemical processes may be quite complicated, requiring the use of spectroelectrochemical techniques.

3.1. Zn–TRP

Because of its well behaved properties, the Zn–TRP species provides the most representative example in the M–TRP series. This complex exhibits the characteristic absorption bands of $Zn^{II}TPyP$ at 430 nm (Soret band), 562 and 606 nm (Q bands), and of the $[Ru^{II}(bipy)_2Cl]^+$ moieties at 298 nm (bipy, $\pi \rightarrow \pi^*$), 450–490 nm (Ru^{II}-to-bipy charge transfer envelope) and 358 nm (see Fig. 6A). One additional band associated with the Ru^{II}-to-pyP MLCT transition has been found at 466 nm, using resonance Raman spectroscopy [48].

Typical cyclic voltammograms [47] of the Zn–TRP complex are shown in Fig. 7. Starting from 0.00 V and scanning in the direction of more positive potentials, an intense reversible wave can be observed at $E_{1/2} = 0.92$ V followed by another wave at 1.50 V. The oxidation of the [Zn–TRP] complex at $E_{1/2} = 0.92$ V leads to the decay of the MLCT band in the 450–490 nm region, splitting the bipy $\pi \rightarrow \pi^*$ band at 298 nm into two peaks at 306 and 318 nm, and shifting the Soret band to 434 nm (see Fig. 6). The spectroscopic changes are consistent with the oxidation of the

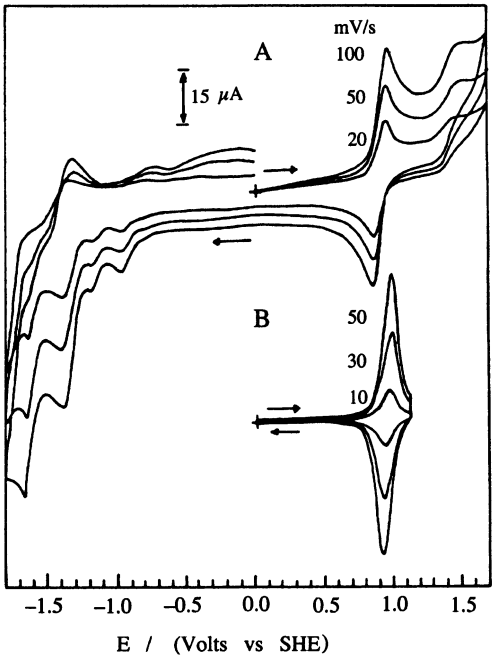

Fig. 7. (A) Cyclic voltammograms of $[Zn–TRP](TFMS)_4$ (9.9×10^{-4} M) in DMF (0.10 M $TEAClO_4$) obtained using a platinum disc electrode. (B) CV of a 1.8×10^{-8} mol cm^{-2} film adsorbed on a glassy carbon disc electrode, in 0.026 M acetate buffer (pH 4.7) and 0.25 M LiTFMS.

ruthenium–bipyridine complexes. At 1.5 V, the oxidation process leads to the decay of the Soret and Q bands, with minor changes in the bipy $\pi \rightarrow \pi^*$ band, indicating the oxidation of the porphyrin ring. In the negative potential region, the voltammograms exhibit two reversible waves at $E_{1/2} = -0.93$ and -1.14 V, followed by two intense waves at -1.35 and -1.67 V. The reduction of the $Zn^{II}TPyP$ moiety at -0.9 V leads to a bathochromic shift of the Soret and Q bands to 444, and 580 and 626 nm, respectively, with many simultaneous isosbestic points. The spectroscopic changes differ dramatically from those previously reported for the reduction centered at the porphyrin ring, and are consistent with a strong involvement of the metal center in the reduced species. In contrast, the second reduction process at –1.1 V leads to the decay of the Soret and Q bands, and to the rise of new absorption bands at 492 and 756 nm, characteristic of a porphyrin radical anion. At -1.4 V, the intensities of the bipy $\pi \rightarrow \pi^*$ band at 298 nm and the porphyrin π-radical anion band at 492 nm decay to about one half of their original values, indicating the reduction of one bipyridine ligand in each complex and the second reduction of the porphyrin center. At -1.70 V, the band at 298 nm disappears, being replaced by a broad band at 338 nm, indicating the complete reduction of the bipyridine ligands to the corresponding radical anions.

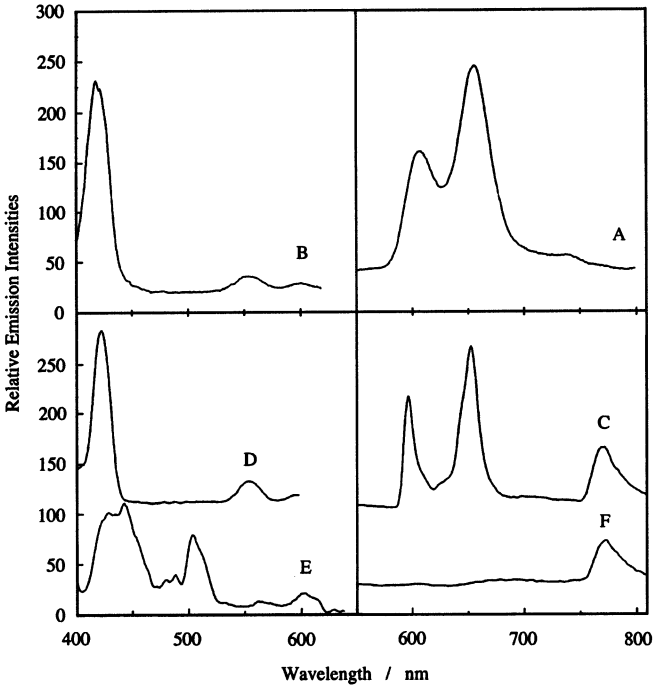

Fig. 8. (A) Emission ($\lambda_{exc} = 422$ nm) and (B) excitation ($\lambda_{em} = 655$ nm) spectra of an 8×10^{-7} M ethanol solution of $[Zn–TRP](TFMS)_4$ at room temperature. (C) Emission ($\lambda_{exc} = 422$ nm); (D) excitation ($\lambda_{em} = 655$ nm); (E) excitation ($\lambda_{em} = 778$ nm) and (F) emission ($\lambda_{exc} = 450$ nm) spectra of an 2×10^{-6} M glassy ethanol solution at 77 K.

The room temperature excitation and emission spectra of the tetraruthenated–zinc porphyrin are shown in Figs. 8A and B. The complex exhibits two well-defined fluorescence bands at 606 and 655 nm, corresponding to the singlet-singlet $Q_{0\text{-}0}$ and $Q_{1\text{-}0}$ transitions within the Zn–TPyP group. The excitation spectrum obtained by monitoring the intensity of these two fluorescence bands does not reproduce the absorption spectrum of the tetraruthenated complex, displaying exclusively the absorption profile of the zinc porphyrin group, represented by the Soret, $Q_{0\text{-}0}$ and $Q_{1\text{-}0}$ bands at 417, 554 and 601 nm, respectively. The time-resolved spectrum of the tetraruthenated porphyrin is very similar to those previously reported in the literature [49] for the triplet excited states of related porphyrins, confirming that the low-lying excited state of the polymetallic system is centered on the zinc porphyrin moiety. There is no evidence of excitation of the porphyrin via the peripheral $[Ru(bpy)_2Cl]^+$ groups, indicating that in solution, at room temperature, the energy transfer from the peripheral groups to the porphyrin center singlet state is not efficient. In addition, the lack of emission from the $[Ru(bipy)_2Cl]^+$ moieties suggests that the corresponding excited states are also rapidly deactivated.

At low temperatures (77 K) the emission spectrum (see Figs. 8C and D) of the corresponding ethanol glass exhibits two narrow $Q_{0\text{-}0}$ and $Q_{0\text{-}1}$ emission bands at 597 and 652 nm, and another band at 770 nm. This new band has been assigned to the triplet state emission ($T_{0\text{-}0}$) by comparison with the phosphorescence spectrum of similar porphyrins. The excitation spectrum obtained by monitoring the 652 nm porphyrin singlet emission is similar to that observed at room temperature; however when the 770 nm porphyrin triplet emission is monitored, the resulting excitation profile is quite different (see Figs. 8E and F). In this case, the charge transfer absorptions around 500 and 450 nm associated with the peripheral ruthenium complexes become evident, indicating the occurrence of energy transfer from $[Ru(bipy)_2Cl]^+$ triplet states to the lowest energy triplet state of the zinc porphyrin. This conclusion is corroborated by the fact that the emission spectrum obtained by excitation at 450 nm, i.e. in the MLCT band of the ruthenium complexes, exhibits essentially the porphyrin phosphorescence emission.

The triplet emission bands of the $[Ru(bipy)_2Cl(L)]^+$ complexes, where L = pyridine or 4-acetylpyridine, occur at 660 and 653 nm, respectively. By comparison, the emission band of the peripheral $[Ru(bipy)_2Cl]^+$ groups is expected around 660 nm, corresponding to a very weak emission band observed at 680 nm. Therefore, the excited triplet level of the peripheral ruthenium groups is higher than the porphyrin triplet level, allowing the occurrence of intramolecular energy transfer.

In fact, at low temperatures, two mechanisms are responsible for the population of the low-lying triplet state of Zn–TPyP: one involving singlet–triplet intersystem crossing within the porphyrin and another involving direct energy transfer from the ruthenium charge-transfer excited state. The expected decrease in the rates of thermal relaxation processes for the Zn–TPyP and $[Ru(bipy)_2Cl]^+$ excited states should increase the quantum yields of intersystem crossing, allowing the triplet–triplet energy transfer within the polymetallic complex.

3.2. Co–TRP

The incorporation of a cobalt ion in TRP leads to a particularly interesting system for redox purposes, allowing the exploitation of the electrochemical activity of this metal ion in a supramolecular porphyrin environment. The corresponding cyclic voltammograms show, in addition to the TRP waves, a broad reduction wave around -0.5 V, not observed in the Zn–TRP analogue. The spectroelectrochemical changes in this region have revealed a surprising sequence of events, as shown

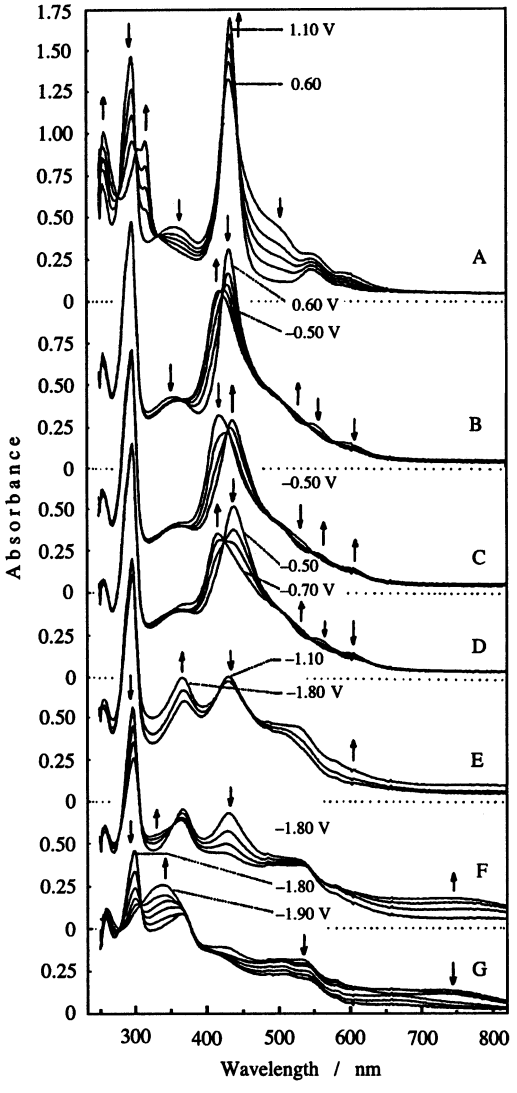

Fig. 9. Spectroelectrochemistry of 1 mM $[CoTRP](TFMS)_4$ in DMF solution containing 0.10 M $TEAPF_6$ in the potential range 1.10 to -1.90 V vs. SHE.

in Fig. 9, which are consistent with the occurrence of three successive redox steps. Initially, at -0.5 V, the Soret band shifts from 434 to 424 nm followed by another shift to 440 nm as a function of time; and finally it moves back to 418 nm when the potential was moved to -0.7 V. The three spectroelectrochemical changes proceed with well defined isosbestic points, and the typical porphyrin-like spectrum is maintained while the absorption bands associated with the ruthenium complexes remain practically unchanged. For this reason, the three successive processes were ascribed to the stepwise reduction of Co^{III}–TPyP to Co^{II}–TPyP to Co^{I}–TPyP and to Co^{0}TPyP.

3.3. Ni–TRP

In the case of the [Ni–TRP] [51,52] complex the cyclic voltammograms are shown in Fig. 10. Contrasting behavior has been observed for the Ni–TRP first and second reduction waves at -0.80 and -0.97 V, which differ appreciably from the those of the typical species, e.g. $[Ni–TMPyP]^{4+}$ at -0.37 and -0.73 V, reflecting the influence of the π-back-bonding interactions from the attached Ru^{II} groups. The

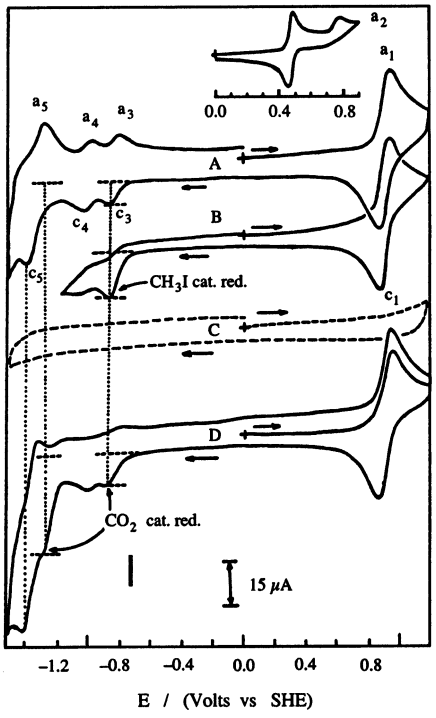

Fig. 10. Cyclic voltammograms (50 mV s^{-1}) of: (A) [Ni–TRP](TFMS)$_4$ (1.1 mmol dm^{-3}) in DMF, $TEAClO_4$ 0.10 mol dm^{-3}, under an argon atmosphere; (B) in the presence of 16.2 mmol dm^{-3} of CH_3I; (C) of an electrolyte solution saturated with CO_2; and (D) of the complex solution saturated with CO_2. Inset: Voltammogram of a 1.1 mmol dm^{-3} solution of the complex in acetonitrile, $TEAClO_4$ 0.10 mol dm^{-3}.

existence of Ni(I) character in the reduced complexes generated at −0.80 V, has been investigated by adding methyl iodide. Ni(I) species, exhibiting a d^9 configuration, and CH_3 are isolobal species and should react readily, in contrast to the Ni(II) species. As a matter of fact, methyl iodide enhances by a factor of 2, the cathodic current at −0.80 V. No such effect has been observed when the porphyrin anion presents essentially a π-radical character [53,54]. Therefore, the results indicate significant Ni(I) character for the reduced tetraruthenated nickel porphyrin species. In the presence of CO_2, there is a small increase in the reduction wave at −0.80 V but a great intensification at −1.30 V. According to the voltammograms, the major product of the CO_2 reduction is electrochemically inactive in the range of −1.5 to 1.0 V, and is most probably CO. The peripheral $[Ru(bipy)_2Cl]^+$ groups enhance the catalytic activity of the nickel porphyrin center, by increasing the Ni(I) character of the reduced species.

3.4. Interaction of tetraruthenated porphyrins with DNA

The interaction of TRPs and DNA leads to pronounced changes in the absorp-

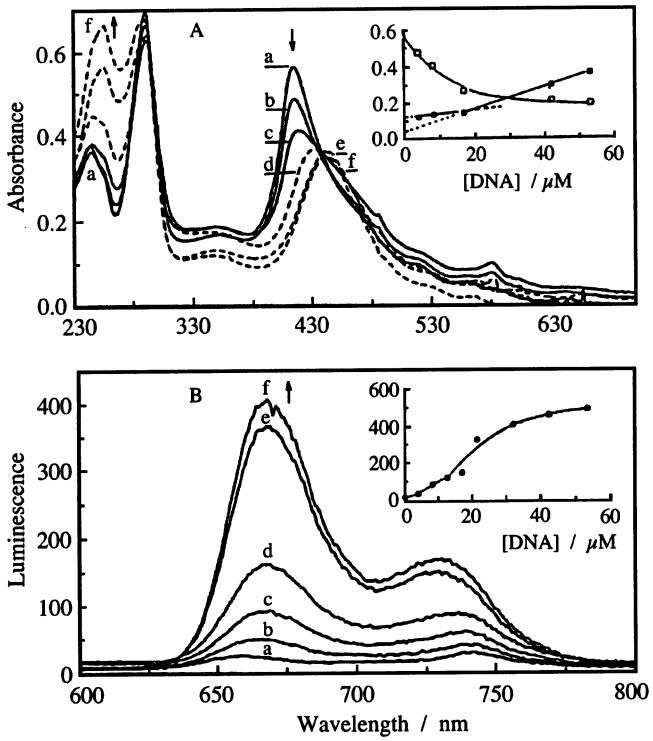

Fig. 11. (A) Absorption and (B) fluorescence spectra of 2.5 μM $[TRP]Cl_4$ in the presence of: (a) 0; (b) 4.2; (c) 8.5; (d) 17 and (f) 53 μM (in nucleotide phosphate) calf thymus DNA, 0.050 M phosphate buffer, pH 7.4; $\lambda_{exc} = 430$ nm. Inset: (A) absorbance vs. [DNA] (□); and (B) corrected luminescence vs [DNA], including additional points.

tion and emission spectra [55], as illustrated in Fig. 11. The optical measurements support the occurrence of two stage binding processes between supercoiled pBR322 ($K_1 = 1.8 \times 10^5$, $K_2 = 4.2 \times 10^4$ $mol^{-1}dm$) or calf thymus DNA ($K_1 = 1.5 \times 10^5$, $K_2 = 2.5 \times 10^4$ mol^{-1} dm) and the modified porphyrin.

Exposure of pBr322 DNA to light, in the presence of H_2TRP leads to single-strand break formation, as determined by the conversion of the supercoiled form of the plasmid into the circular form. Oxidative DNA base damage has been evaluated by the formation of 8-oxo-7,8-dihydro-2′-deoxyguanosine (8-oxodGuo), after irradiation of calf thymus DNA in the presence of the modified porphyrin. The results are coherent with two types of photoinduced mechanisms leading to strand scission activity and 8-oxodGuo formation. Formation of singlet molecular oxygen after H_2TRP excitation has been confirmed from its characteristic near-infrared emission. Mechanistic studies [56] have indicated that the photooxidation mediated by H_2TRP and principally by Zn–TRP occurs predominantly by means of the energy transfer process to dioxygen generating the active species $^1O_2$. A potential application of the tetraruthenated porphyrin in photodynamic therapy has been proposed.

3.5. Supramolecular films

The $[M–TRP]^{4+}$ complexes in the presence of a suitable counter ion, e.g. trifluomethanesulfonate (TFMS) form very homogeneous films onto solid surfaces, by the slow evaporation of methanol solutions [57]. The nature of the polymetallic complex is preserved in the adsorbed films, as can be inferred from its characteristic electronic spectrum, resonance Raman and electrochemical and spectroelectrochemical response.

The electronic spectra of the $[Ni–TRP](TFMS)_4$ films are very similar to those of the molecular species in solution [57]. The films deposited on glassy carbon exhibit a well behaved electrochemical response in aqueous solution, displaying reversible waves at $E° = 0.95$ V, associated with the peripheral ruthenium complexes (see Fig. 12). The full widths at half maximum (FWHM) for the anodic and cathodic waves are 120 and 150 mV, respectively. The peak currents increase linearly as a function of the scan rate, with a small difference in the slopes arising from the non-equivalent FWHM values. These results are consistent with a fast ion diffusion and electron transfer within the film, with a minor repulsive site-to-site interaction, or differences in redox species environment. Because of their bulkiness, the mobility of the molecules within the film should be hindered, such that the direct electron transfer to the electrode resulting from their diffusion is unlikely. The electron transport within the film has been assigned to a self-exchange redox mechanism because in the presence of ferrocyanide ions, no current was observed at its normal oxidation potential, i.e. 0.37 V, during the anodic scan. However, a sharp wave appeared at the beginning of the $Ru^{III/II}$ anodic wave (0.7 V). Therefore, the electrochemical processes are being mediated by the film, which acts as a conduction gate, allowing a unidirectional electron flow from the solution to the electrode.

The results obtained with ferrocyanide ions indicated that the film pores are rather small, with no significant amount of pin-holes and other discontinuities (see Fig. 12). The linear relationship of the peak currents with respect to the scan rates implies that the redox sites are exchanging electrons with the electrode, so that the total surface concentration can be evaluated coulometrically. On the other hand, the high homogeneity observed by scanning electon microscopy (SEM) and the similarity of the solution and film spectra, suggest that the films are formed by compact and homogeneous layers of molecules adsorbed flat onto the electrode surface. Probably, the supermolecules are stacking with the porphyrin rings coplanar to each other in order to maximize the hydrophobic interactions. In this arrangement the ruthenium complexes are close together and generate a molecular wire connecting the electrode surface and the solution. Assuming a molecular area

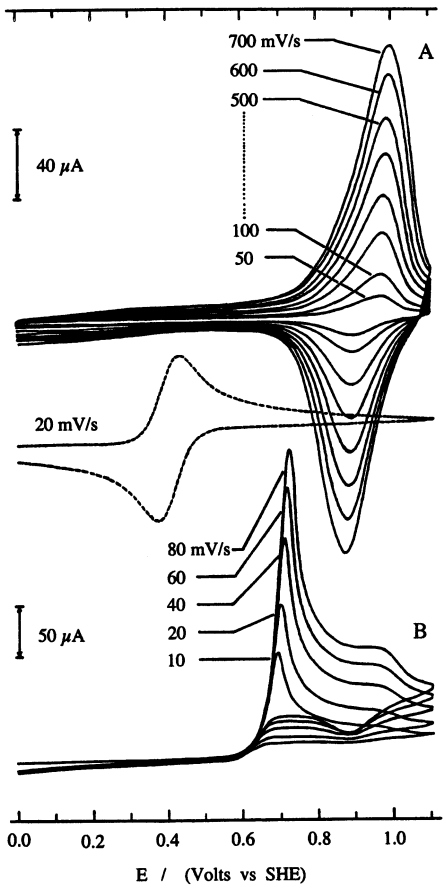

Fig. 12. (A) Cyclic voltammograms of [Ni–TRP](TFMS)$_4$ film on glassy carbon electrode surface, $\Gamma_T = 1.0$ nmol cm^{-2}; in LiTFMS 0.25 M, acetate buffer 0.05 M, pH 4.7. (B) Cyclic voltammograms of $K_4[Fe(CN)_6]$ 5.37 mM in bare electrode (top) and on Ni–TRP modified glassy carbon, $\Gamma_T = 0.74$ nmol cm^{-2} (bottom).

of 400 Å^2, each monolayer should contain around 4×10^{-11} mol cm^{-2}. A typical film on an electrode area of 0.2 cm^2 involves a total of 1×10^{-4} C and is consistent with about 30 monolayers. The electrochemical potential at the film/solution interface is determined by the redox potential of the $Ru^{III/II}$ couple.

The [Zn–TRP](TFMS)$_4$ films [47] exhibit only a narrow emission band at 730 nm (see Fig. 13C), as found in the phosphorescence spectrum in ethanol glass at 77 K, in contrast with the fluorescence spectrum in solution. A remarkable point is that only phosphorescence was observed for the films at room temperature. Their excitation profiles parallel the absorption profiles of Zn–TPyP and [Ru(bipy)$_2$Cl]$^+$ moieties, indicating that the peripheral groups are effectively acting as antennae in the complex. The electronic coupling facilitates the zinc porphyrin singlet to ruthenium complexes triplet state energy transfer, decreasing the fluorescence quantum yield. Also, there is a rapid energy transfer process from the excited [Ru(bipy)$_2$Cl]$^+$ groups to the zinc porphyrin triplet state, competing with the thermal deactivation processes.

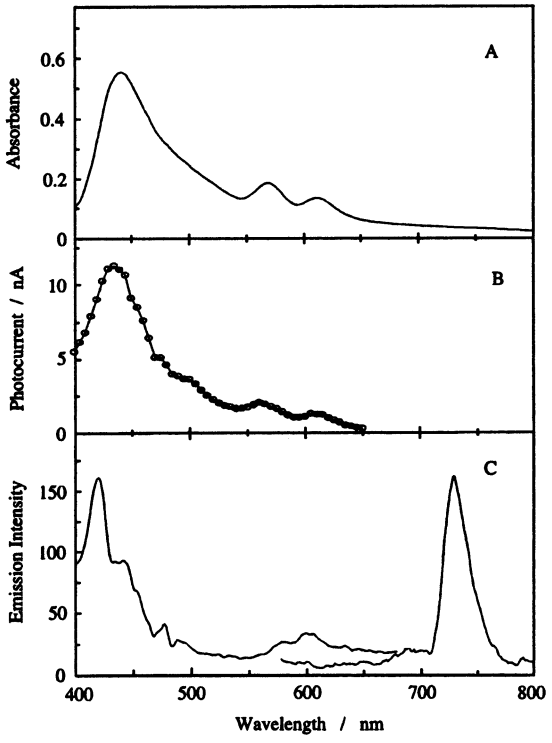

Fig. 13. (A) Electronic spectrum of a film deposited on platinum electrode surface; (B) Photoaction spectrum (average of five measurements) of a $\Gamma_T = 5.9 \times 10^{-9}$ mol cm^{-2} film of [Zn–TRP](TFMS)$_4$ adsorbed onto a glassy carbon electrode in an O_2 saturated aqueous solution containing 0.26 M acetate buffer (pH 4.7) and 0.25 M LiTFMS at $E = 0.22$ V; (C) excitation ($\lambda_{em} = 725$ nm) and emission ($\lambda_{exc} = 422$ nm) spectra of [Zn–TRP](TFMS)$_4$ film on glassy carbon at room temperature.

Another remarkable aspect is related to the photoelectrochemical properties of the [Zn–TRP](TFMS)$_4$ films [47]. When the films are illuminated, a stable photocurrent response is generated, reproducing its absorption profile (see Figs. 3A and B). This result confirms that the $[Ru(bipy)_2Cl]^+$ groups can effectively act as antennae, absorbing light and transferring energy or electrons within the molecular framework at the electrode surface.

Another application is in cases where the sensibility of an electrochemical method is diminished by the slow electron transfer kinetics at the electrode surface. The determination of sulfite is a typical example. As a matter of fact, sulfite has a very slow electron transfer kinetics on the electrode surface such that it does not exhibits any appreciable electrochemical response in the range of 0.6–1.2 V. But the use of a [M–TRP] modified electrode leads to a significant enhancement of the oxidation wave around 1.0 V and the currents are proportional to the substrate concentration, allowing its use for analytical purposes. The [CoTRP](TFMS)$_5$ films are particularly suitable for electrode modification [57,58], possessing good homogeneity, stability and adherence. The Co^{III} films have been successfully employed in the determination of nitrite, sulfite, NADH and dopamine, in flow injection analysis [46,50,57–59]. The glassy carbon electrodes coated with molecular films of the tetraruthenated cobaltporphyrin exhibit enhanced electrochemical response, leading

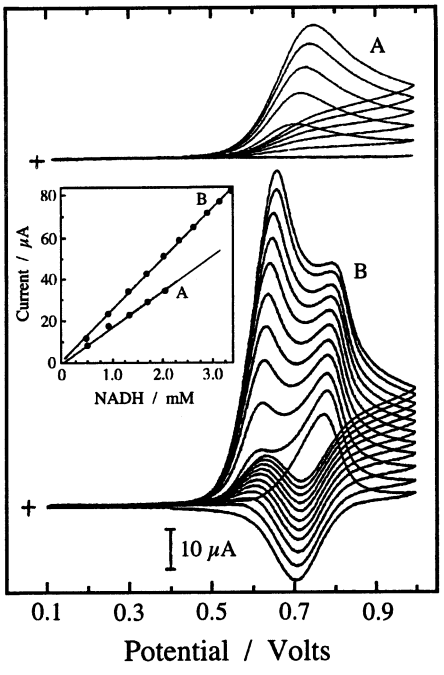

Fig. 14. Cyclic voltammograms of NADH solutions using (A) a bare glassy carbon electrode in the 0.5 to 2.0 mM range and (B) and electrode modified with [CoTRP](TFMS)$_4$, $\Gamma_T = 1.1 \times 10^{-9}$ mol cm^{-2}, in the range 0.5–3.5 mM. Scan rate = 100 mV s^{-1}, acetate buffer 0.05 M (pH 4.7), [LiTFMS] = 0.25 M. Inset: plot of peak currents vs NADH concentrations.

to sharp signals at the onset of the $Ru^{III/II}$ redox wave (ca. 0.70 V). Examples of the determination of NADH at ppb levels, in FIA, are illustrated in Fig. 14 [58].

The $[M–TRP](TFMS)_4$ complexes form homogeneous and adherent films on the glassy carbon surfaces by dip-coating. However, they are gradually lixiviated in the absence of TFMS counter-anion. This problem has been solved by using a new material, constituted by insoluble ion-paired stacked porphyrins [59,60], namely $[M–TRP]^{4+}$ and $[M–TPPS]^{4-}$. The UV–vis absorption (see Fig. 15) and thickness measurements based on AFM have demonstrated that the double layered [Zn–TRP]/[TPPS] films can grow in a linear way, as a function of the number of dippings [60]. The average bilayer thickness is 12.7 Å. The electrostatically assembled Zn–TRP/TPPS films are electrochemically and photoelectrochemically active, exhibiting a photocurrent action spectrum very similar to the UV–vis absorption spectrum of the film.

The electrochemical properties of the [CoTRP]/[ZnTPPS] films have been evaluated in comparison with the dip-coated $[CoTRP](TFMS)_5$ films [59]. The electrodes modified with the double layered material exhibit an electrochemical response very similar to the dip-coated electrodes, however are more stable and can be used for many days under the demanding FIA conditions without loss of sensibility (see Fig. 16). The electrode has provided enhanced and stable signals for analytes such as nitrite and sulfite, and in addition, they are resistant to passivation due to surface fouling. This is one of the major problems affecting solid electrodes for successive amperometric analysis. A typical example is the rapid passivation of bare electrodes employed in the amperometric determination of phenolic compounds. The response of the modified electrode remains almost constant after ten analysis of a 10 μmol dm^{-3} phenol solution, whereas the signal for the bare glassy carbon electrode decreases to about half of its initial intensity.

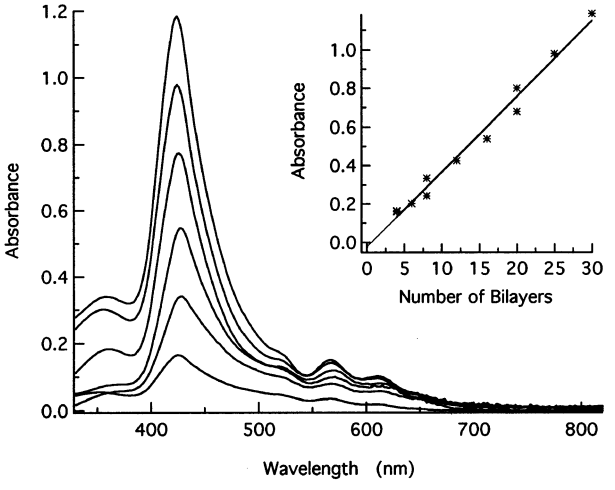

Fig. 15. UV–vis spectra of 4, 8, 16, 20, 25 and 30 bilayer films of [Zn–TRP]/[TPPS] on ITO. Inset: growth of the absorbance as a function of the number of bilayers.

4. New perspectives

Since our initial work on the tetraruthenated porphyrins, an increasing number of possibilities have been devised, by changing the macrocyclic center or the nature of the attached complexes [32–35,61–63]. For instance, a novel series of supramolecular porphyrin species, containing four triangular μ-oxo-ruthenium-acetate clusters [7–12,64], has been recently reported (see Fig. 17).

The tetracluster porphyrin (TCP) represents a dodecanuclear complex with four triangular μ-oxo-ruthenium acetate clusters, $[Ru_3O(Ac)_6(py_2)]^+$ groups, coordinated to the pyridyl N-atoms. The primordial interest in this series is associated with the capability of the ruthenium cluster to undergo multi-step electron transfer in the −1.5 to 2.4 V range, in order to generate the $Ru^{IV}Ru^{IV}Ru^{III}$, $Ru^{IV}Ru^{III}Ru^{III}$, $Ru^{III}Ru^{III}Ru^{III}$, $Ru^{III}Ru^{III}Ru^{II}$ and $Ru^{III}Ru^{II}Ru^{II}$ species. The attachment of this versatile redox species to the porphyrin center may enhance its redox or electrocat-

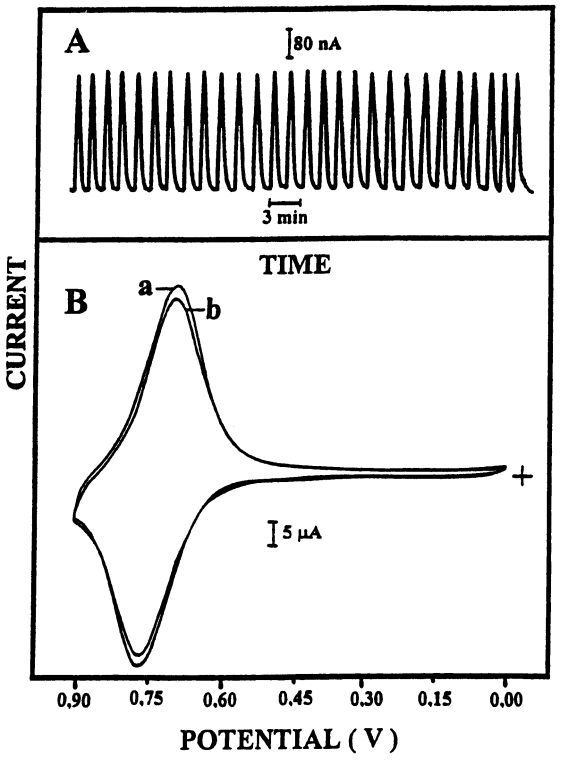

Fig. 16. (A) FIA amperometric responses to consecutive 100 μl injections of nitrite (10^{-5} mol dm^{-3}) and (B) cyclic voltammograms of a glassy carbon electrode modified with [CoTRP]/[ZnTPPS] bilayered film in the presence of the carrier solution (a) before and (b) after 1 h of continuous nitrite analysis by FIA. Conditions for FIA: $E = +0.90$ V, flow rate = 0.8 cm^3 min^{-1}; cyclic voltammetry scan rate = 100 mV s^{-1}.

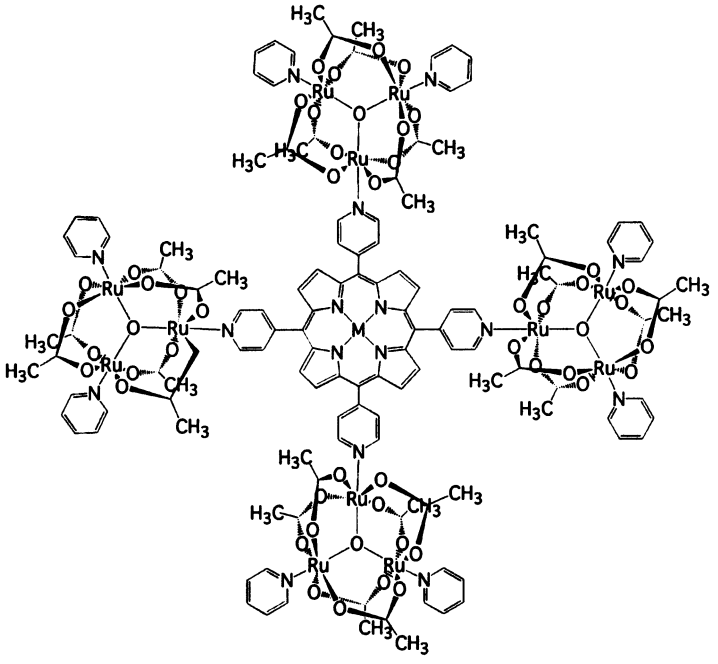

Fig. 17. Structural representation of the tetracluster porphyrin (TCP) supermolecule.

alytic activity, in a wide range of applied potentials. In addition, the TCP complex can also associate very strongly with anionic species, such as tetrasulfonatephthalocyaninecopper(II), forming electrostatically assembled materials.

Acknowledgements

The support from FAPESP, CNPq and PADCT is gratefully acknowledged.

References

[1] J.-M. Lehn, Angew. Chem. Int. Ed. Engl. 27 (1988) 89.
[2] H.E. Toma, A.B.P. Lever, Inorg. Chem. 25 (1986) 176.
[3] H.E. Toma, P.R. Auburn, E.S. Dodsworth, M.N. Golovin, A.B.P. Lever, Inorg. Chem. 26 (1987) 4257.
[4] H.E. Toma, R.L. Sernaglia, Talanta 40 (1993) 515.
[5] H.E. Toma, P.S. Santos, S.G. Camera, R.L. Sernaglia, Spectrosc. Lett. 30 (1997) 507.
[6] C. Hidalgo-Luangdilok, A.B. Bocarsly, Inorg. Chem. 29 (1990) 2894.
[7] A.D.P. Alexiou, H.E. Toma, J. Chem. Res. S (1997) 338.
[8] H.E. Toma, A.D.P. Alexiou, J. Chem. Res. S (1995) 134.
[9] H.E. Toma, A.D.P. Alexiou, J. Braz. Chem. Soc. 6 (1995) 267.

[10] H.E. Toma, M.A.L. Olive, Polyhedron 13 (1994) 2647.
[11] H.E. Toma, C. Cipriano, J. Electroanal. Chem. 346 (1993) 261.
[12] H.E. Toma, P.S. Santos, C. Cipriano, Spectrosc. Lett. 21 (1988) 909.
[13] S. Campagna, G. Denti, G. De Rosa, L. Sabatino, M. Ciano, V. Balzani, Inorg. Chem. 28 (1989) 2565.
[14] L. De Cola, V. Balzani, F. Barigelletti, L. Flamigni, P. Belser, A.v. Zelewsky, M. Frank, F. Vogtle, Inorg. Chem. 32 (1993) 5228.
[15] G. Denti, S. Campagna, L. Sabatino, S. Serroni, M. Ciano, V. Balzani, Inorg. Chem. 29 (1990) 4750.
[16] S. Campagna, G. Denti, S. Serroni, M. Ciano, V. Balzani, Inorg. Chem. 30 (1991) 3728.
[17] G. Denti, S. Campagna, L. Sabatino, S. Serroni, M. Ciano, V. Balzani, Inorg. Chim. Acta 176 (1990) 175.
[18] G. Denti, S. Campagna, S. Serroni, M. Ciano, V. Balzani, J. Am. Chem. Soc. 114 (1992) 2944.
[19] S. Campagna, G. Denti, S. Serroni, M. Ciano, A. Juris, V. Balzani, Inorg. Chem. 31 (1992) 2982.
[20] F. Barigelletti, L. Flamigni, V. Balzani, J. -P. Collin, J. -P. Sauvage, A. Sour, E.C. Constable, A.M.W.C. Thompson, J. Am. Chem. Soc. 116 (1994) 7692.
[21] J.-P. Collin, S. Guillerez, J.-P. Sauvage, F. Barigelletti, L. De Cola, L. Flamigni, V. Balzani, Inorg. Chem. 31 (1992) 4112.
[22] J.-P. Collin, P. Laine, J.-P. Launay, J.-P. Sauvage, A. Sour, J. Chem. Soc. Chem. Commun. (1993) 434.
[23] E.C. Constable, M.D. Ward, J. Chem. Soc. Dalton Trans. (1990) 1405.
[24] V. Grosshenny, A. Harriman, R. Ziessel, Angew. Chem. Int. Ed. Engl. 34 (1995) 1100.
[25] G.S. Hanan, C.R. Arana, J.-M. Lehn, D. Fenske, Angew. Chem. Int. Ed. Engl. 34 (1995) 1122.
[26] J.-P. Sauvage, J.-P. Collin, J.-C. Chambron, S. Guillerez, C. Coudret, Chem. Rev. 94 (1994) 993.
[27] L.M. Vogler, C. Franco, S.W. Jones, K.J. Brewer, Inorg. Chim. Acta 221 (1994) 55.
[28] Comprehensive Supramolecular Chemistry, Pergamon Press, New York, 1996.
[29] F.C. Anson, C.N. Shi, B. Steiger, Acc. Chem. Res. 30 (1997) 437.
[30] C.N. Shi, F.C. Anson, Inorg. Chem. 31 (1992) 5078.
[31] B. Steiger, F.C. Anson, Inorg. Chem. 36 (1997) 4138.
[32] J.L. Sessler, V.L. Capuano, A.K. Burrell, Inorg. Chim. Acta 204 (1993) 91.
[33] L. Flamigni, N. Armaroli, F. Barigelletti, V. Balzani, J.P. Collin, J.O. Dalbavie, V. Heitz, J.P. Sauvage, J. Phys. Chem. B 101 (1997) 5936.
[34] A. Harriman, F. Odobel, J.P. Sauvage, J. Am. Chem. Soc. 117 (1995) 9461.
[35] J.-P. Collin, A. Harriman, V. Heitz, F. Odobel, J.-P. Sauvage, J. Am. Chem. Soc. 116 (1994) 5679.
[36] J.P. Collin, V. Heitz, J.P. Sauvage, Tetrahedron Lett. 32 (1991) 5977.
[37] H.E. Toma, K. Araki, Proceedings of the 6th Brazilian Symposium on Electrochemistry and Electroanalalysis, São Paulo, Brazil, 1988, p. 183.
[38] H.E. Toma, K. Araki, J. Chem. Res. S (1990) 82.
[39] H.E. Toma, K. Araki, Inorg. Chim. Acta 179 (1991) 293.
[40] K. Araki, P.S. Santos, H.E. Toma, Spectrosc. Lett. 26 (1993) 1417.
[41] B. Steiger, F.C. Anson, Inorg. Chem. 34 (1995) 3355.
[42] C.N. Shi, B. Steiger, F.C. Anson, Pure Appl. Chem. 67 (1995) 319.
[43] C.N. Shi, F.C. Anson, Inorg. Chim. Acta 225 (1994) 215.
[44] H.E. Toma, K. Araki, J. Coord. Chem. 30 (1993) 9.
[45] A. Juris, V. Balzani, F. Barigelletti, S. Campagna, P. Belser, A. von Zelewisky, Coord. Chem. Rev. 84 (1988) 85.
[46] K. Araki, A.L. Araujo, M.M. Toyama, M. Franco, C.M.N. Azevedo, L. Angnes, H.E. Toma, J. Porphyr. Phthalocyanines 2 (1998) 467.
[47] K. Araki, H.E. Toma, J. Photochem. Photobiol. 83 (1994) 245.
[48] K. Araki, P.S. Santos, L.F.C.D. Oliveira, H.E. Toma, Spectrosc. Lett. 28 (1995) 119.
[49] J. Rodriguez, C. Kirmaier, D. Holten, J. Am. Chem. Soc. 111 (1989) 6500.
[50] K. Araki, L. Angnes, C.M.N. Azevedo, H.E. Toma, J. Electroanal. Chem. 397 (1995) 205.
[51] K. Araki, H.E. Toma, J. Chem. Res. S (1994) 290.
[52] K. Araki, H.E. Toma, J. Chem. Res. M (1994) 1501.

[53] K.M. Kadish, M.M. Franzen, B.C. Han, C. Araullo-McAdams, D. Sazou, J. Am. Chem. Soc. 113 (1991) 512.
[54] A.M. Stolzenberg, M.T. Stershic, J. Am. Chem. Soc. 110 (1988) 5397.
[55] J. Onuki, A.V. Ribas, M.H.G. Medeiros, K. Araki, H.E. Toma, L.H. Catalani, P. DiMascio, Photochem. Photobiol. 63 (1996) 272.
[56] J.-L. Ravanat, J. Cadet, K. Araki, H.E. Toma, M.H.G. Medeiros, P.D. Mascio, Photochem. Photobiol. 68 (1998) 698.
[57] K. Araki, L. Angnes, H.E. Toma, Adv. Mater. 7 (1995) 554.
[58] L. Angnes, C.M.N. Azevedo, K. Araki, H.E. Toma, Anal. Chim. Acta 329 (1996) 91.
[59] C.M.N. Azevedo, K. Araki, L. Angnes, H.E. Toma, Electroanalysis 10 (1998) 467.
[60] K. Araki, M.J. Wagner, M.S. Wrighton, Langmuir 12 (1996) 5393.
[61] E. Alessio, M. Macchi, S.L. Heath, L.G. Marzilli, Inorg. Chem. 36 (1997) 5614.
[62] J.P. Collin, A. Harriman, V. Heitz, F. Odobel, J.P. Sauvage, Coord. Chem. Rev. 148 (1996) 63.
[63] C.M. Drain, F. Nifiatis, A. Vasenko, J.D. Batteas, Angew. Chem. Int. Ed. Engl. 37 (1998) 2344.
[64] H.E. Toma, K. Araki, E.O. Silva, Monatshefte Chem. 129 (1998) 975.